



Published in final edited form as:

Magn Reson Med. 2011 August ; 66(2): 555–564. doi:10.1002/mrm.22800.

Combined Use of T2-weighted MRI and T1-weighted DCE-MRI in the Automated Analysis of Breast Lesions

Neha Bhooshan, M.Eng, Maryellen Giger, Ph.D., Li Lan, MS, Hui Li, Ph.D., Angelica Marquez, Akiko Shimauchi, M.D., and Gillian M. Newstead, M.D.

University of Chicago, Department of Radiology, 5841 S. Maryland Ave, MC2026, Chicago, IL 60637

Abstract

A multi-parametric computer-aided diagnosis (CADx) scheme that combines information from T1-weighted DCE-MRI and T2-weighted MRI was investigated using a database of 110 malignant and 86 benign breast lesions. Automatic lesion segmentation was performed, and three categories of lesion features (geometric, T1-weighted DCE, and T2-weighted) were automatically extracted. Stepwise feature selection was performed considering only geometric features, only T1-weighted DCE features, only T2-weighted features, and all features. Features were merged with Bayesian artificial neural networks, and diagnostic performance was evaluated by ROC analysis. With leave-one-lesion-out cross-validation, an AUC value of 0.77 ± 0.03 was achieved with T2-weighted-only features, indicating high diagnostic value of information in T2-weighted images. AUC values of 0.79 ± 0.03 and 0.80 ± 0.03 were obtained for geometric-only features and T1-weighted DCE-only features, respectively. When all features were considered, an AUC value of 0.85 ± 0.03 was achieved. We observed p -values of 0.0006, 0.023, and 0.0014 between the {geometric-only, T1-weighted DCE-only, and T2-weighted-only features} and all features conditions, respectively. When ranked, the p -values satisfied the Holm-Bonferroni multiple-comparison test; thus, the improvement of multi-parametric CADx was statistically significant. A CADx scheme that combines information from T1-weighted DCE and T2-weighted MRI may be advantageous over conventional T1-weighted DCE-MRI CADx.

Keywords

breast cancer; computer-aided diagnosis; T1-weighted dynamic contrast enhanced magnetic resonance imaging; T2-weighted magnetic resonance imaging

Introduction

Dynamic contrast-enhanced magnetic resonance (DCE-MR) imaging of the breast with gadolinium-based contrast agents now is accepted widely as a potential adjunct to

Contact information Ph: 773-834-5099, Fax: 773-702-0371, bhooshan@uchicago.edu.

M.L.G. is a stockholder in R2 Technology/Hologic and receives royalties from Hologic, GE Medical Systems, MEDIAN Technologies, Riverain Medical, Mitsubishi and Toshiba. It is the University of Chicago Conflict of Interest Policy that investigators disclose publicly actual or potential significant financial interest that would reasonably appear to be directly and significantly affected by the research activities.

conventional imaging modalities such as mammography and ultrasonography (US).¹⁻³ The diagnosis in DCE-MR imaging is based on morphology and contrast material enhancement velocity. Breast carcinomas generally show a faster and stronger signal intensity increase after a bolus injection of gadolinium-based contrast agent than most benign lesions and normal breast tissue. In addition, morphology assessment of internal lesion heterogeneity and margins is also key in making the final diagnosis.

While the sensitivity of breast MR imaging is encouraging, its specificity is variable. Peters et al. conducted a meta-analysis on 44 valid studies and obtained an overall sensitivity of 0.90 and an overall specificity of 0.72 in the diagnostic accuracy of breast MRI.⁴ The limited specificity of contrast-enhanced MR imaging may be attributed to the fact that several types of benign breast lesions also can show strong contrast agent enhancement.⁵

The relatively low specificity of T1-weighted DCE-MRI of breast cancer has led researchers to investigate different approaches including examination of T2-weighted images alongside T1-weighted DCE-MRI images in their standard interpretation of breast MRI cases.⁶⁻⁸ Kuhl et al. found that the analysis of T2-weighted sequences during interpretation were a useful adjunct in the differential diagnosis of benign and malignant lesions. For example, fibroadenomas, a benign lesion that can exhibit similar contrast agent enhancement to that of malignant lesions on T1-weighted DCE-MRI, had a high signal intensity (SI) on T2-weighted images in comparison to malignant lesions, which generally have low SI on T2-weighted images.

However, MRI assessment of breast cancer cases may be hindered by inter- and intra-observer variations, labor-intensive interpretation methods, and limited clinical interpretation guidelines.⁹⁻¹² To aid radiologists in diagnostic classification, various investigators are developing computerized image analysis methods for characterization.¹³ Computer-aided diagnosis (CADx) schemes were initially developed for mammography and ultrasound¹⁴ and recently have been extended to breast MRI, specifically T1-weighted DCE-MRI.¹⁵⁻²⁰

To the best of our knowledge, few CADx studies have investigated multi-parametric MR analysis, i.e. combining information from both T2-weighted and T1-weighted DCE-MRI for distinguishing between malignant and benign lesions. Thus, the purpose of this study was twofold. First, we investigated the computerized analysis of T2-weighted MRI images in distinguishing malignant and benign breast lesions. Second, we evaluated whether including T2-weighted computer features in our current DCE-MRI CADx scheme could improve the diagnostic performance of the overall CADx system.

Materials and Methods

Database

The study was an IRB-approved HIPAA-compliant study in which the requirement for informed consent was waived. A review of MR examinations performed at the University of Chicago Medical Center (UCMC) between November 2008 and August 2009 yielded 86 benign breast lesions (no cysts) and 110 malignant breast lesions in 161 female patients

(mean age, 61 yrs \pm 15; range, 28–86 years). Benign lesions included fibrocystic change (16/86), fibroadenomas (45/86), papillomas (4/86), and other atypical benign disease (21/86). Malignant lesions included invasive ductal carcinoma (66/110), invasive lobular carcinoma (11/110), ductal carcinoma in situ (24/110), and other atypical malignant disease (9/110). Figure 1 shows the distribution of lesion volumes (in cubic centimeters). All lesions used in the study were examined and reported by experienced radiologists and pathologists, and all cases were reviewed at a multidisciplinary breast cancer management conference.

The patients were scanned in prone position using a standard double 16-channel breast coil (Invivo breast coil, Philips Healthcare, Amsterdam, The Netherlands) on a 1.5T whole-body scanner (Philips Healthcare, Amsterdam, The Netherlands). The patient was first scanned with a T2-weighted turbo spin echo (TSE) sequence (2000/319 [repetition time msec/echo time msec], 90° flip angle). Images were then acquired using a T1-weighted 3D gradient echo (THRIVE) sequence with fat suppression (5.5/2.7 [repetition time msec/echo time msec], 12° flip angle). After the acquisition of the precontrast series, gadolinium-diethylenetriamine penta-acetic acid (Gd-DTPA) contrast agent was given intravenously with a fixed dose of 20cc followed by a 20-mL saline flush. Six post-contrast series were obtained at 60-second time intervals. The T1-weighted DCE and T2-weighted MR images were acquired with the same scan parameters – in-plane spatial resolution (0.74mm \times 0.74mm), axial plane acquisition, slice thickness (2mm), number of slices (200 slices), initial scan position, patient position (prone position), and matrix size (range from 432 \times 432 to 512 \times 512 pixels).

Segmentation

A fuzzy *c*-means (FCM) clustering based method was used to automatically segment the 3D breast tumors in the DCE-MR images and is described in detail elsewhere.¹⁸ This scheme included six steps. A region of interest (ROI) was first selected by a human operator. The post-contrast ROI series were normalized by dividing the pixel value at each post-contrast voxel by the value at the corresponding pre-contrast voxel. After the FCM clustering method was applied, the lesion membership map was dichotomized with an empirically determined threshold to partition the whole ROI into lesion and non-lesion components. Then, a 3D connected-component labeling operation reduced false-positive voxels followed by a hole-filling function to yield the final 3D contour or segmentation of the lesion. Since the T1-weighted DCE and T2-weighted MR images were acquired with the same scan parameters, the segmentation obtained on the T1 image data was overlaid on the T2-weighted images.

Computer-Extracted Features

Mathematical lesion descriptors in this study were grouped into four types of features: geometric features; morphological features; kinetic features; and enhancement-variance kinetics features.

Geometric features were based on the lesion outline from the lesion segmentation algorithm and did not incorporate pixel value data in the calculation. The features were sphericity, irregularity, and lesion volume in cubic millimeters; sphericity quantifies the compliance of a lesion to a sphere and irregularity measures the roughness of the lesion contour surface.²¹

Morphological features consist of texture features and spiculation features. Texture features were calculated from the gray-level co-occurrence matrix (GLCM).^{22,23} The element (i, j) in a directional GLCM represents the joint probability $p(i, j)$ of the occurrence of gray levels i and j in the two paired image elements with an offset of r along the direction θ in the image(s). A voxel in 3D breast MR images was surrounded by 26 neighboring voxels in 13 independent directions, thereby giving 13 directional GLCMs. However, the voxels were anisotropic in breast MR images due to the poorer inter-slice spatial resolution compared to the intra-slice spatial resolution. A linear interpolation was thus employed before the construction of directional GLCMs to yield isotropic voxels. A non-directional GLCM was obtained by summing all the directional GLCMs. Fourteen texture features were extracted from the non-directional GLCM to quantify different textural characteristics of a lesion, such as homogeneity, gray-level dependence, brightness, and randomness. The specific features included contrast, correlation, difference entropy, difference variance, energy, entropy, homogeneity, maximum correlation coefficient, sum average, sum entropy, sum variance, variance, and two information measures of correlation.²³ The spiculation features included radial gradient index (RGI), margin sharpness, and variance of margin sharpness. RGI is based on the radial gradient of the pixels within the lesion and its local environment.²¹ Margin sharpness is the mean gradient magnitude along the margin of the lesion while variance of margin sharpness is the variance of the image gradient at the lesion margin.²¹ Since the morphological features include image data, they were generated for both T1-weighted DCE (specifically, the first post-contrast images) and T2-weighted images. In addition, the mean of the signal intensity of the T2-weighted images was also calculated.

Kinetic features quantify the enhancement kinetics of the breast lesions on T1-weighted DCE images and aim to reveal the physiologic process of the uptake and washout of the contrast agent during the imaging time. First, the characteristic kinetic curve (CKC) of a lesion was automatically identified by FCM clustering.¹⁹ The signal-time curves obtained from each voxel in a segmented 3D lesion were clustered into several prototypal curves, and the curve with the highest initial enhancement was selected as the characteristic curve representative of the lesion. Seven kinetic features were then extracted from the CKC including maximum contrast enhancement, time to peak, uptake rate, washout rate, curve shape index, enhancement at the 1st post-contrast time frame, and signal enhancement ratio.¹⁹

Enhancement-variance kinetics features characterize the time course of the spatial variance of the enhancement within the lesion on T1-weighted DCE images. Similar to the kinetic features, the maximum enhancement-variance, time to peak, the increasing rate of spatial variance, and the decreasing rate of spatial variance were determined.²⁰

In summary, three categories of features were analyzed. T1-weighted DCE features included morphological features (texture and spiculation), kinetics, and enhancement-variance kinetics while T2-weighted features included morphological features (texture and spiculation). The last category was the geometric features which were based solely on the segmented contour of the lesion. A summary of features and their descriptions are given in Table 1.

Feature Selection and Performance Evaluation

To select the effective set of lesion features, step-wise feature selection was performed by linear discriminant analysis using the Wilks lambda criterion as the cost function in a leave-one-lesion-out (LOLO) fashion.²⁴ Four conditions for diagnostic classification were investigated: (i) considering only geometric features, (ii) considering only T1-weighted features, (iii) considering only T2-weighted features, and (iv) considering all features (T2-weighted, T1-weighted DCE, geometric) combined. Once the feature histogram was generated, the cut-off threshold was empirically set at 50% of the frequency of the most chosen feature, and features whose frequency were greater than the threshold were selected for the classification task. The number of features was limited to six or less to preserve the robustness of the classification method and reduce the risk of overtraining.

The selected features were merged with Bayesian artificial neural network (BANN) classifier to yield computer-estimated probability of malignancy (PM).²⁵ The ROCKIT software was used to evaluate the classifier's performance using LOLO cross-validation, and the area under the ROC curve (AUC) was used as the performance metric.^{26–28} The *p*-values were calculated between conditions {i, ii, iii} and iv; the Holm-Bonferroni *t* test with the overall α -level set at 0.05 was used for multiple comparisons statistical testing.²⁹ Figure 2 summarizes the overall automatic analysis scheme for condition (iv) in which all features (T2-weighted, T1-weighted DCE, geometric) were considered.

Results

Figure 3 shows example analysis including the segmentation and characteristic kinetic curve of an invasive ductal carcinoma (IDC) grade 2 lesion on subtracted first post-contrast T1-weighted DCE and T2-weighted MR images. The lesion has high SI on the T1-weighted DCE MRI but appears hypointense on the T2-weighted image. Figure 4 shows the same analysis including the segmentation and characteristic kinetic curve of benign fibroadenoma. The lesion also has high SI on the T1-weighted DCE MRI but appears hyperintense on the T2-weighted image.

Figure 5 shows the feature selection histogram for the conditions in which only T1-weighted DCE features were considered and only T2-weighted features were considered. When all features (T2-weighted, T1-weighted DCE, and geometric) were considered, two T2-weighted features (homogeneity and sum average), three T1-weighted DCE features (RGI, enhancement-variance time to peak, and signal enhancement ratio) and one geometric feature (irregularity) were selected. The relationship between irregularity and T1-weighted DCE RGI can be seen in Figure 6. As expected, malignant lesions tend to have large irregularity and small RGI values, demonstrating the general spiculation of malignant lesions. Similarly, the T2-weighted RGI values were usually small for malignant lesions, which are also inclined to have large values for the maximum correlation coefficient feature as seen in Figure 7.

Although RGI and homogeneity were both chosen in the T2-weighted-only features and T1-weighted DCE-only features conditions, when grouped together in the all features condition, the T1-weighted DCE RGI and the T2-weighted homogeneity features were chosen. Figure

8 depicts the homogeneity values for T1-weighted DCE and T2-weighted features. The Pearson correlation between the T2-weighted and T1-weighted DCE values for RGI and homogeneity were 0.67 and 0.72, respectively, with p -value < 0.0001 for both.

The selected features and performance in terms of AUC are shown in Table 2, and the corresponding ROC curves from leave-one-lesion-out analyses are plotted in Figure 9. We achieved AUC values of 0.79 ± 0.03 , 0.80 ± 0.03 , and 0.77 ± 0.03 for the geometric-only features, T1-weighted DCE-only features and T2-weighted-only features, respectively. When all geometric, T1-weighted features, and T2-weighted features were considered within the feature selection algorithm (“all features”), an AUC value of 0.85 ± 0.03 was obtained using the selected features.

The p -value between the performance of geometric-only features and that of “all features” was 0.006 while the p -value between the performance of T1-weighted DCE-only features and that of “all features” was 0.023. The p -value between the performance of the T2-weighted-only features and that of “all features” was 0.0014. When ranked, these p -values satisfy the Holm-Bonferroni correction for multiple comparisons, indicating that there is a statistically significant difference between considering only one type of feature and considering all features.

Using a cut-off threshold of 0.20 for the computer-estimated probability of malignancy, the sensitivity and specificity for the geometric-only features were 98% and 10% and for the T1-weighted DCE-only features, they were 95% and 32%, respectively. The sensitivity and specificity for the T2-weighted-only features were 98% and 12% and for the all features, they were 96% and 35%, respectively.

As noted earlier, both RGI and homogeneity for T1-weighted DCE and T2-weighted features were selected in the separate modality analyses; however only the T1-weighted DCE RGI and the T2-weighted homogeneity features were chosen when all features from all modalities were considered. When T1-weighted DCE homogeneity was replaced by T2-weighted homogeneity in the all features condition, the AUC decreased from 0.85 to 0.82. Similarly, when T2-weighted RGI was replaced by T1-weighted DCE RGI in the all features condition, the AUC of 0.85 decreased to 0.84. However, these decreases were not found to be statistically significant.

Discussion

Based solely on the computerized characterization of the T2-weighted morphological characteristics of the lesion, an AUC value of 0.77 ± 0.03 was achieved in differentiating between malignant and benign lesions. Its performance was similar to the geometric-only AUC of 0.79 ± 0.03 and T1-weighted DCE-only AUC of 0.80 ± 0.03 . Thus, simply using T2-weighted features shows promise in diagnostic classification.

When stepwise feature selection was run on all features (T2-weighted, T1-weighted DCE, and geometric), two T2-weighted features (homogeneity and sum average) were selected along with three T1-weighted DCE features and one geometric feature, indicating that the T2-weighted features performed strongly enough among the T1-weighted DCE and

geometric features to be selected. The resulting AUC of 0.85 ± 0.03 was significantly higher than the single feature type AUC values.

Overall, specificity increased by 3% and sensitivity increased by 1% when all geometric, T1-weighted DCE, and T2-weighted features were input to the feature selection algorithm and subsequent classification analysis, as compared to using only T1-weighted DCE features. To better understand how T2-weighted analysis aided the CADx scheme, we can consider the example lesions in Figures 3 and 4. In Figure 3, the malignant lesion has an irregular shape (thus a high PM of 0.59 using geometric features) but the kinetic curve is persistent. Since signal enhancement ratio was a selected T1-weighted DCE feature, it follows that the T1-weighted DCE PM was 0.34. However, the PM from the T2-weighted was 0.68 and the overall PM was 0.75. Thus, the T2-weighted features helped the CADx scheme to correctly identify the lesion as malignant. For the benign lesion in Figure 4, the PMs for the geometric and T1-weighted DCE features were 0.48 and 0.56 respectively but the T2-weighted PM was 0.24, pulling the overall computer-estimated PM to 0.31. These examples illustrate that when lesions have unclear kinetics (malignant lesion with persistent kinetics or benign lesions with rapid uptake/washout kinetics), analysis of the T2-weighted images may help the CADx scheme better distinguish malignant and benign lesions.

As noted earlier, the Pearson correlation coefficients between the T2-weighted and T1-weighted DCE values for the RGI and homogeneity features were moderately high with statistical significance. However, as seen in Figure 8, it seems that the image information in the T1-weighted DCE MRI versus the information inherent in the T2-weighted images of the same lesion appear different. Additionally, as evident by the decrease in AUC values when using the T1-weighted DCE instead of T2-weighted values for these two features in the “all-features” performance, the T2-weighted may have better diagnostic accuracy than the T1-weighted DCE with respect to specific morphological characteristics.

Interestingly, the T2-weighted mean SI feature (single AUC value of 0.53) was not selected in the T2-weighted-only feature selection; however two GLCM-based texture features, homogeneity and maximum correlation coefficient with AUC values of 0.72 and 0.70 respectively, were chosen. This may indicate that the texture analysis conducted by the computer may perform better and be more efficient than simply performing visual assessment of SI on T2-weighted MR images.

There are several limitations to the study. During feature selection, the feature sets were generally stable across the leave-one-lesion-out iterations, as seen in Figure 5, yielding minimal bias from using the dataset for both leave-one-lesion-out feature selection and leave-one-lesion-out classification performance evaluation. We also restricted the number of features to a maximum of six features to preserve the robustness of the classification method and reduce the risk of overtraining. However, validation on an independent data set is necessary for an unbiased evaluation. An additional limitation of the study is that we only analyzed cases performed at our institution and did not include cases from outside institutions.

Image brightness (i.e., hypo- or hyper-intensity) on the T2-weighted images was not truly evaluated. Signal intensity can vary from scan to scan depending on gain settings but it was not normalized in our study. Normalization with respect to adjacent tissue or control ROI for the T2-weighted images would allow for true assessment of the hypointensity or hyperintensity of the lesion. No additional spatial registration was used between the T2 and T1-weighted images and between the different T1-weighted acquisitions. We did not observe any substantial motion artifacts in our database; however, it is expected that image registration would improve the results of our analysis, and will be considered in future work.

Despite these limitations, we find this study promising in that the T2-weighted MR images appear to have yielded additional morphological information beyond that from the T1-weighted MR images, and thus are potentially useful in improving diagnostic accuracy, as evident by the performance of the RGI and homogeneity features. A CADx scheme that combines features extracted from both T1-weighted DCE-MR and T2-weighted MR images may be advantageous over the conventional T1-weighted DCE-MRI CADx in the task of classifying malignant and benign breast lesions.

Acknowledgments

The authors are grateful to Weijie Chen, Ph.D., for help with the breast CADx workstation. This work is supported in parts by NIH R33-113800 and P50-CA125183, an NIH Medical Scientist Training Program (MSTP) grant, DOE grant DE-FG02-08ER6478, NIH S10 RR021039 and P30 CA14599, and DOD grant W81XWH-10-1-0216.

References

1. Boetes C, Mus RD, Holland R, Barentsz JO, Strijk SP, Wobbes T, Hendriks JH, Ruys SH. Breast tumors: comparative accuracy of MR imaging relative to mammography and US for demonstrating extent. *Radiology*. 1995; 197:743–747. [PubMed: 7480749]
2. Kac1 GM, Liu P, Debatin JF, Garzoli E, Caduff RF, Krestin GP. Detection of breast cancer with conventional mammography and contrast-enhanced MR imaging. *Eur Radiol*. 1998; 8:194–200. [PubMed: 9477265]
3. Schelfout K, Van Goethem M, Kersschot E, Colpaert C, Schelfhout AM, Leyman P, Verslegers I, Biltjes I, Van Den Haute J, Gillardin JP, Tjalma W, Van Der Auwera JC, Buytaert P, De Schepper A. Contrast-enhanced MR imaging of breast lesions and effect on treatment. *Eur J Surg Oncol*. 2004; 30:501–507. [PubMed: 15135477]
4. Peters N, Borel Rinkes I, Zuithoff N, Mali W, Moons K, Peeters P. Meta-Analysis of MR Imaging in the Diagnosis of Breast Lesions. *Radiology*. 2008; 246:116–124. [PubMed: 18024435]
5. Piccoli CW. Contrast-enhanced breast MRI: factors affecting sensitivity and specificity. *Eur Radiol*. 1997; 7:S281–S288.
6. Kuhl C, Klaschik S, Mielcarek P, Gieseke J, Wardelmann E, Schild H. Do T2-weighted Pulse Sequences Help with the Differential Diagnosis of Enhancing Lesions in Dynamic Breast MRI? *J Mag Reson Img*. 1999; 9:187–196.
7. Santamaría G, Velasco M, Bargalló X, Caparrós X, Farrús B, Luis Fernández P. Radiologic and pathologic findings in breast tumors with high signal intensity on T2-weighted MR images. *Radiographics*. 2010; 30:533–548. [PubMed: 20228333]
8. Torheim G, Godtliebsen F, Axelson D, Kvistad KA, Haraldseth O, Rinck PA. Feature extraction and classification of dynamic contrast-enhanced T2*-weighted breast image data. *IEEE Trans Med Img*. 2001; 20:1293–1301.
9. Mussurakis S, Buckley DL, Coady AM, Turnbull LW, Horsman A. Observer variability in the interpretation of contrast enhanced MRI of the breast. *British J of Rad*. 1996; 69:1009–1016.

10. Ballon DJ, Trenta LRL, Hadar O, Abramson A, Dershaw DD. Observer variability and applicability of BIRADS terminology for breast MR imaging: Invasive carcinomas as focal masses. *AJR*. 2001; 177:551–557. [PubMed: 11517046]
11. Birdwell R, Ikeda D, O’Shaughnessy K, Sickles E. Mammographic characteristics of 115 missed cancers later detected with screening mammography and the potential utility of computer-aided detection. *Radiology*. 2001; 219:192–202. [PubMed: 11274556]
12. Jiang Y, Nishikawa RM, Schmidt RA, Toledano AY, Doi K. Potential of computer-aided diagnosis to reduce variability in radiologists’ interpretations of mammograms depicting microcalcifications. *Radiology*. 2001; 220:787–794. [PubMed: 11526283]
13. Giger ML, Chan H-P, Boone J. Anniversary paper: History and status of CAD and quantitative image analysis: The role of Medical Physics and AAPM. *Med Phys*. 2008; 35:5799–5820. [PubMed: 19175137]
14. Horsch K, Giger ML, Vybony CJ, Lan L, Mendelson EB, Hendrick RE. Multi-modality computer-aided diagnosis for the classification of breast lesions: observer study results on an independence clinical dataset. *Radiology*. 2006; 240:357–368. [PubMed: 16864666]
15. Vomweg TW, Buscema M, Kauczor HU, Teifke A, Intraligi M, Terzi S, Heussel CP, Achenbach T, Rieker O, Mayer D, Thelen M. Improved artificial neural networks in prediction of malignancy of lesions in contrast-enhanced MR-mammography. *Med Phys*. 2003; 30:2350–2359. [PubMed: 14528957]
16. Leinsinger G, Schlossbauer T, Scherr M, Lange O, Reiser M, Wismüller A. Cluster analysis of signal-intensity time course in dynamic breast MRI: does unsupervised vector quantization help to evaluate small mammographic lesions? *Eur Rad*. 2006; 16:1138–1146.
17. Bhooshan N, Giger ML, Jansen SA, Li H, Lan L, Newstead GM. Cancerous breast lesions on dynamic contrast-enhanced MR images: Computerized characterization for image-based prognostic markers. *Radiology*. 2010; 254:680–690. [PubMed: 20123903]
18. Chen W, Giger ML, Bick U. A fuzzy c-means (FCM) based approach for computerized segmentation of breast lesions in dynamic contrast-enhanced MR images. *Acad Radiol*. 2006; 13:63–72. [PubMed: 16399033]
19. Chen W, Giger ML, Bick U, Newstead GM. Automatic identification and classification of characteristic kinetic curves of breast lesions on DCE-MRI. *Medical Physics*. 2006; 33:2878–2887. [PubMed: 16964864]
20. Chen W, Giger ML, Lan L, Bick U. Computerized interpretation of breast MRI: Investigation of enhancement-variance dynamics. *Med Phys*. 2004; 31:1076–1082. [PubMed: 15191295]
21. Gilhuijs KGA, Giger ML, Bick U. Automated analysis of breast lesions in three dimensions using dynamic magnetic resonance imaging. *Med Phys*. 1998; 25:1647–1654. [PubMed: 9775369]
22. Gibbs P, Turnbull LW. Textural analysis of contrast-enhanced MR images of the breast. *Magn Reson in Med*. 2003; 50:92–98. [PubMed: 12815683]
23. Chen W, Giger ML, Li H, Bick U, Newstead GM. Volumetric texture analysis of breast lesions on contrast-enhanced magnetic resonance images. *Magn Reson in Med*. 2007; 58:562–571. [PubMed: 17763361]
24. Johnson, RA.; Wichern, DW. *Applied Multivariate Statistical Analysis*. 3rd ed. Englewood Cliffs, NJ: Prentice-Hall; 1992.
25. Kupinski MA, Edwards DC, Giger ML, Metz CE. Ideal observer approximation using Bayesian classification neural networks. *IEEE Trans Med Img*. 2001; 20:886–899.
26. Metz CE. ROC methodology in radiologic imaging. *Invest Radiol*. 1986; 21:720–733. [PubMed: 3095258]
27. Metz CE, Herman BA, Shen J. Maximum likelihood estimation of receiver operating characteristic ROC curves from continuously-distributed data. *Stat Med*. 1998; 17:1033–1053. [PubMed: 9612889]
28. Metz CE, Herman BA, Roe CA. Statistical comparison of two ROC-curve estimates obtained from partially-paired datasets. *Med Decision Making*. 1998; 18:110–121.
29. Holm S. A simple sequentially rejective multiple test procedure. *Scand. J. Statist*. 1979; 6:65–70.

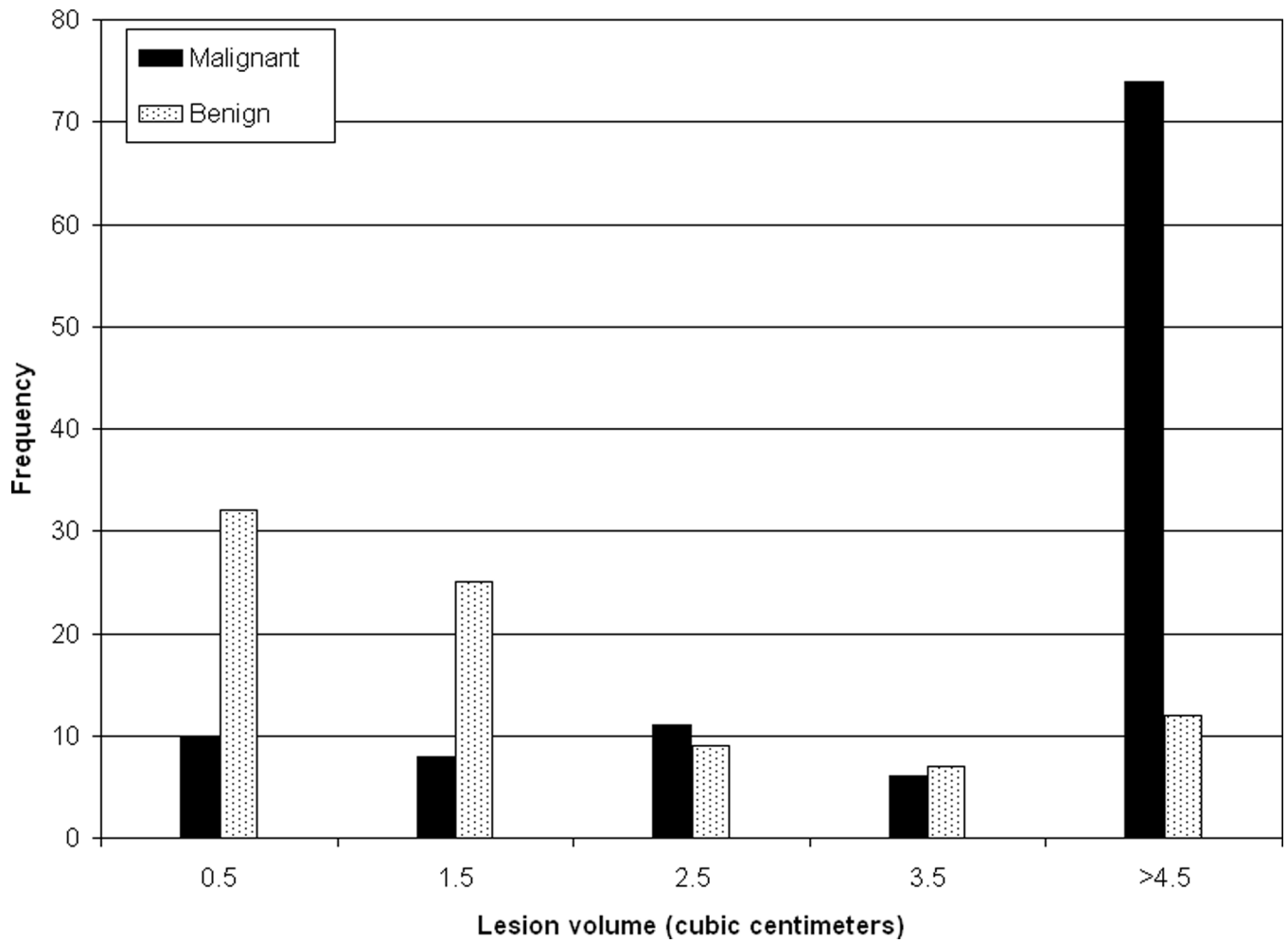


Figure 1. Histogram of volume of lesions (in cubic centimeters) in study database of 110 malignant and 86 benign lesions.

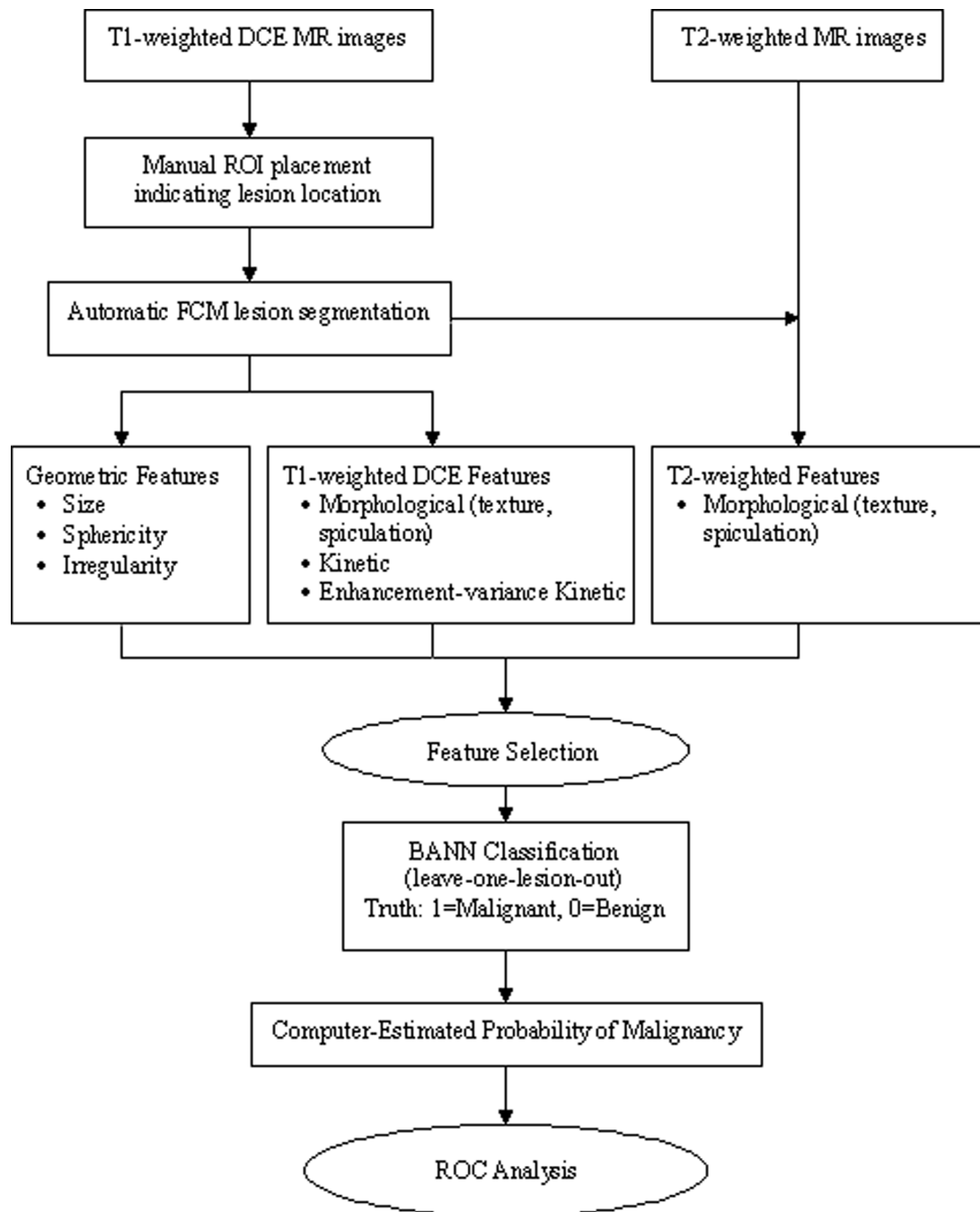
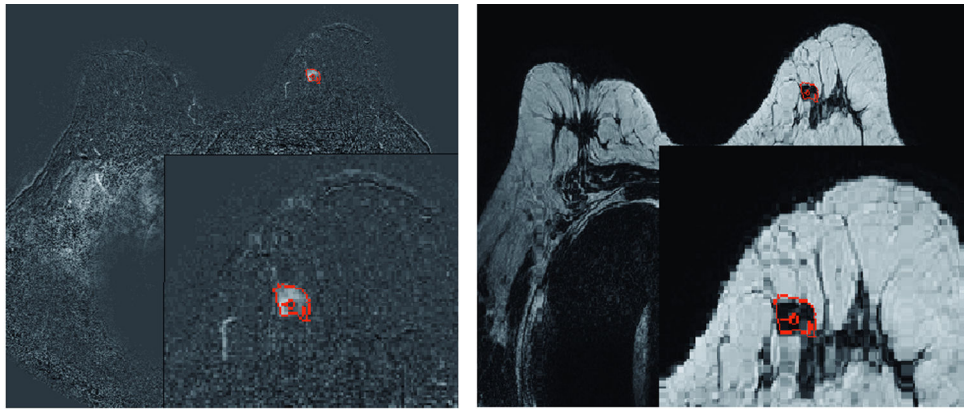


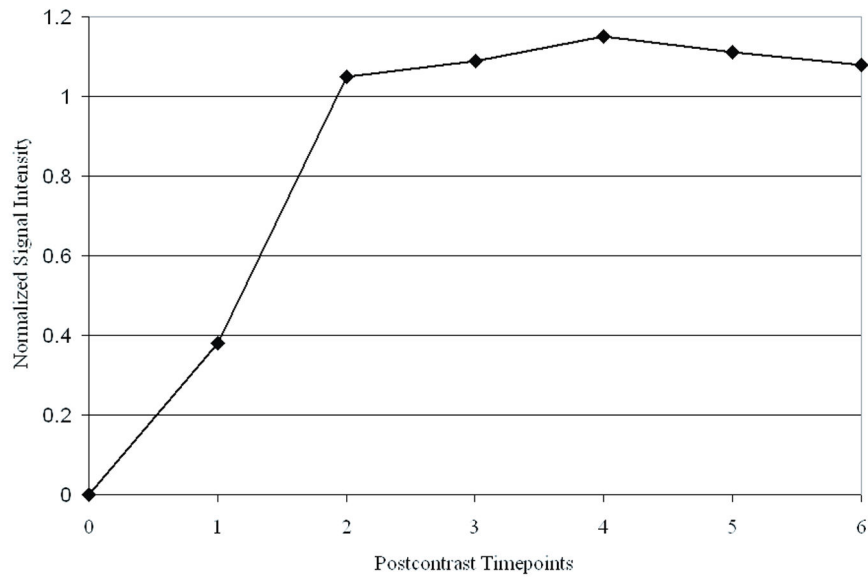
Figure 2. Scheme of automated analysis of breast lesions using T1-weighted DCE and T2-weighted MRI in which all features (geometric, T1-weighted DCE, and T2-weighted) features were considered (iv).



T1-weighted DCE image

T2-weighted image

(a)

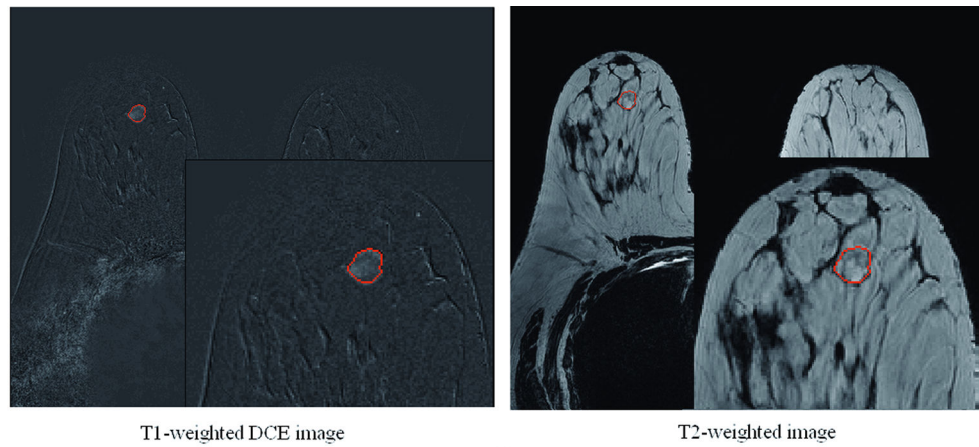


(b)

Condition	Computer-Estimated Probability of Malignancy
Geometric	0.59
T1-weighted DCE	0.34
T2-weighted	0.68
"All features"	0.75

(c)

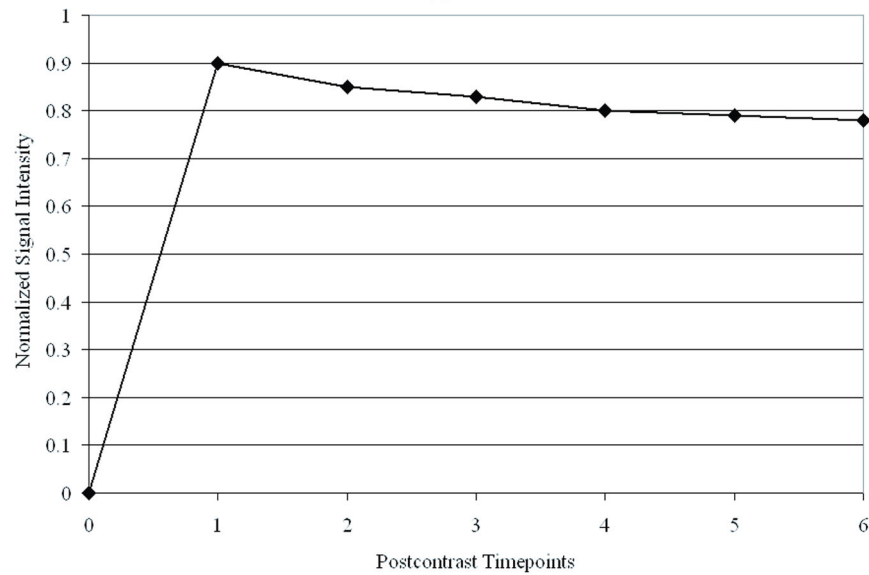
Figure 3. Example malignant lesion (invasive ductal carcinoma grade 2) with (a) segmentations on subtracted first post-contrast T1-weighted DCE and T2-weighted images, (b) signal intensity curve from T1-weighted DCE images, and (c) computer-estimated probabilities of malignancy for four conditions.



T1-weighted DCE image

T2-weighted image

(a)

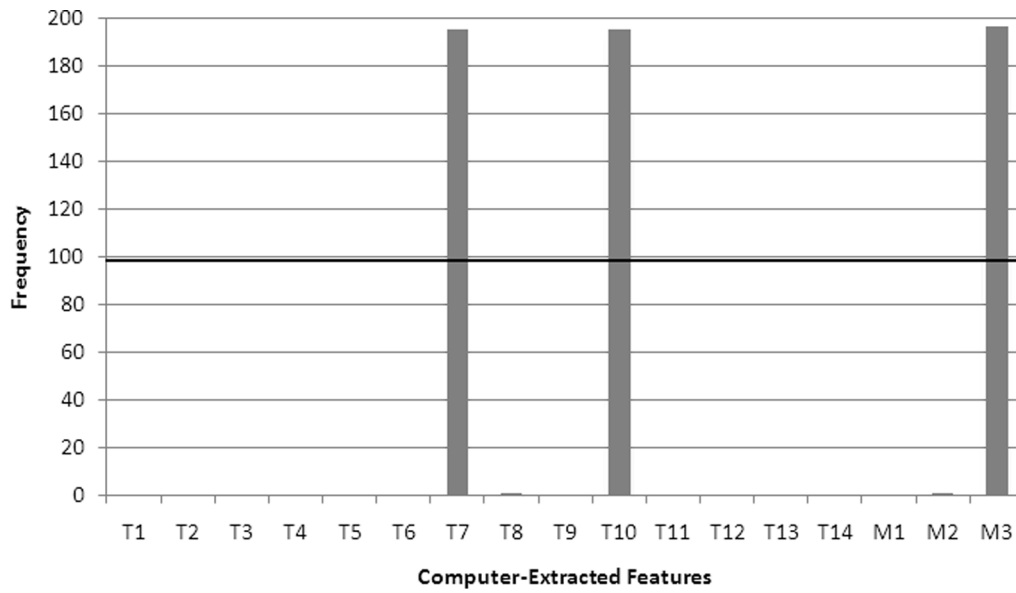


(b)

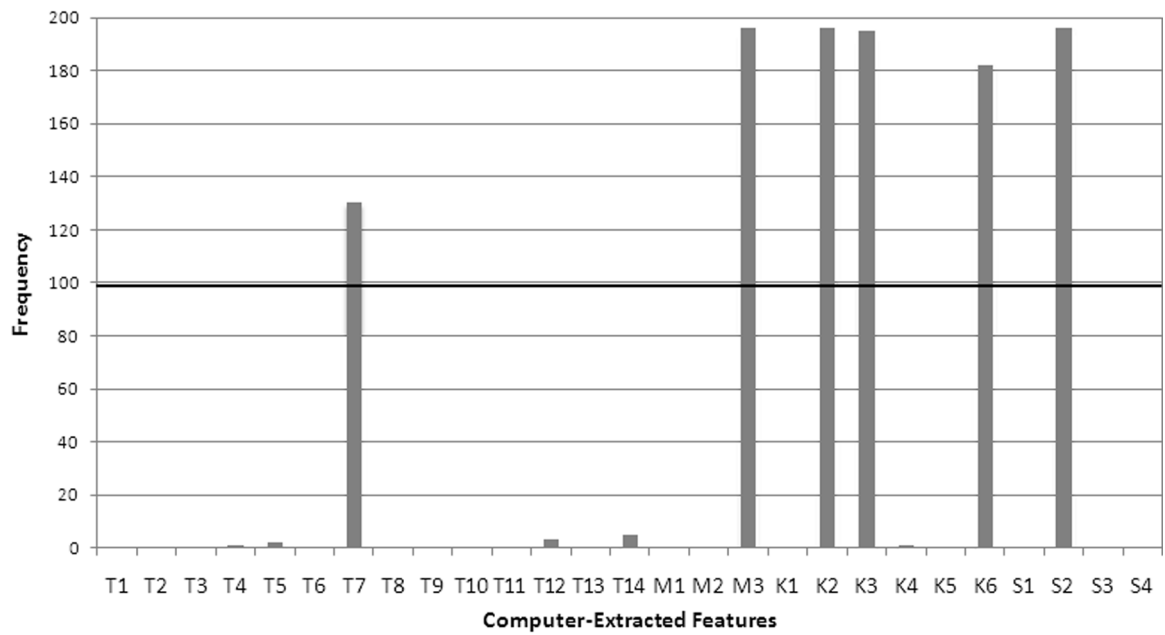
Condition	Computer-Estimated Probability of Malignancy
Geometric	0.48
T1-weighted DCE	0.56
T2-weighted	0.24
"All features"	0.31

(c)

Figure 4. Example benign lesion (fibroadenoma) with (a) segmentations on subtracted first post-contrast T1-weighted DCE and T2-weighted images, (b) signal intensity curve from T1-weighted DCE images, and (c) computer-estimated probabilities of malignancy for four conditions.



(a)



(b)

Figure 5. Histogram of features generated from leave-one-lesion-out stepwise feature selection for (a) T2-weighted features and (b) T1-weighted DCE features.

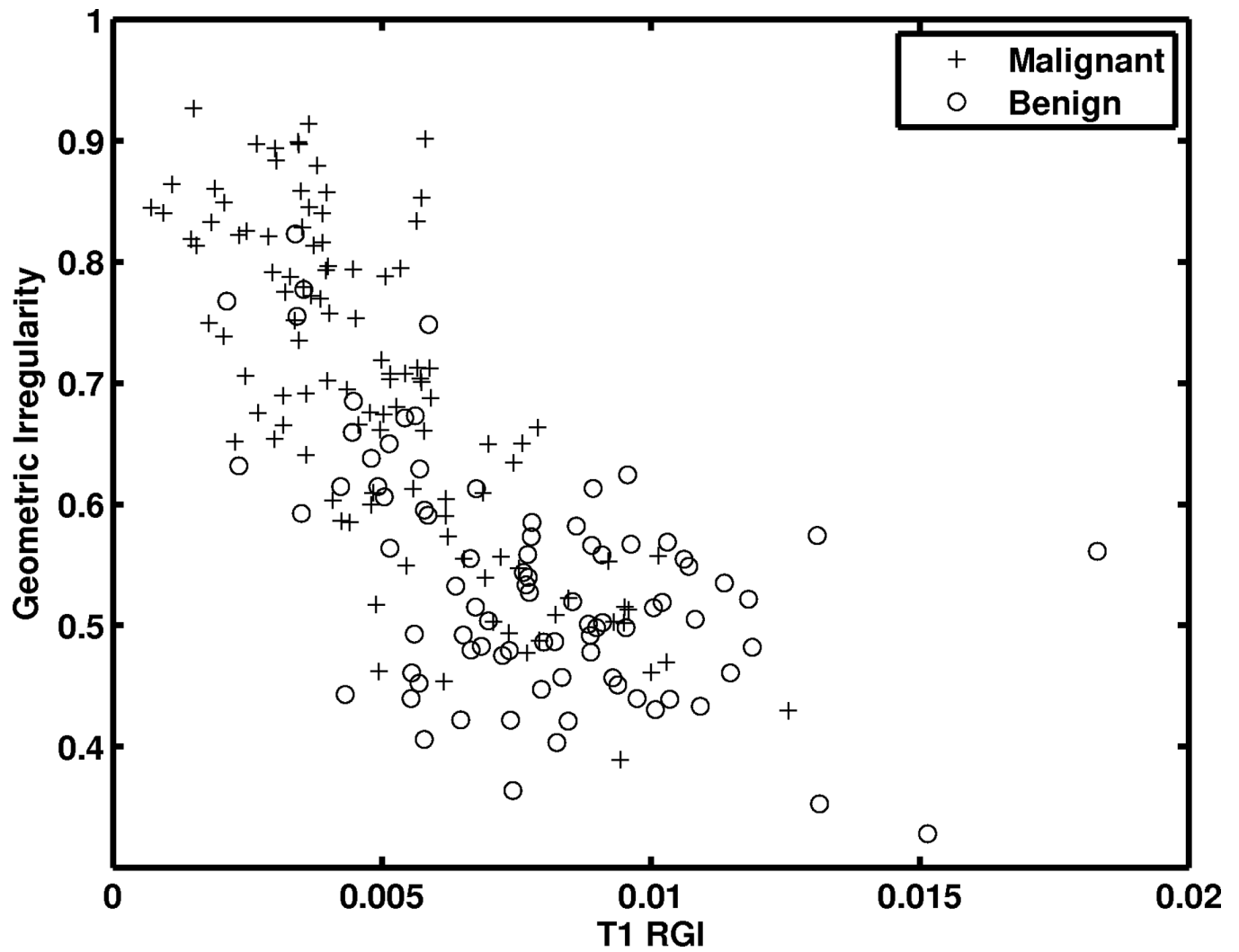


Figure 6.
Relationship between T1-weighted DCE RGI feature and geometric irregularity feature.

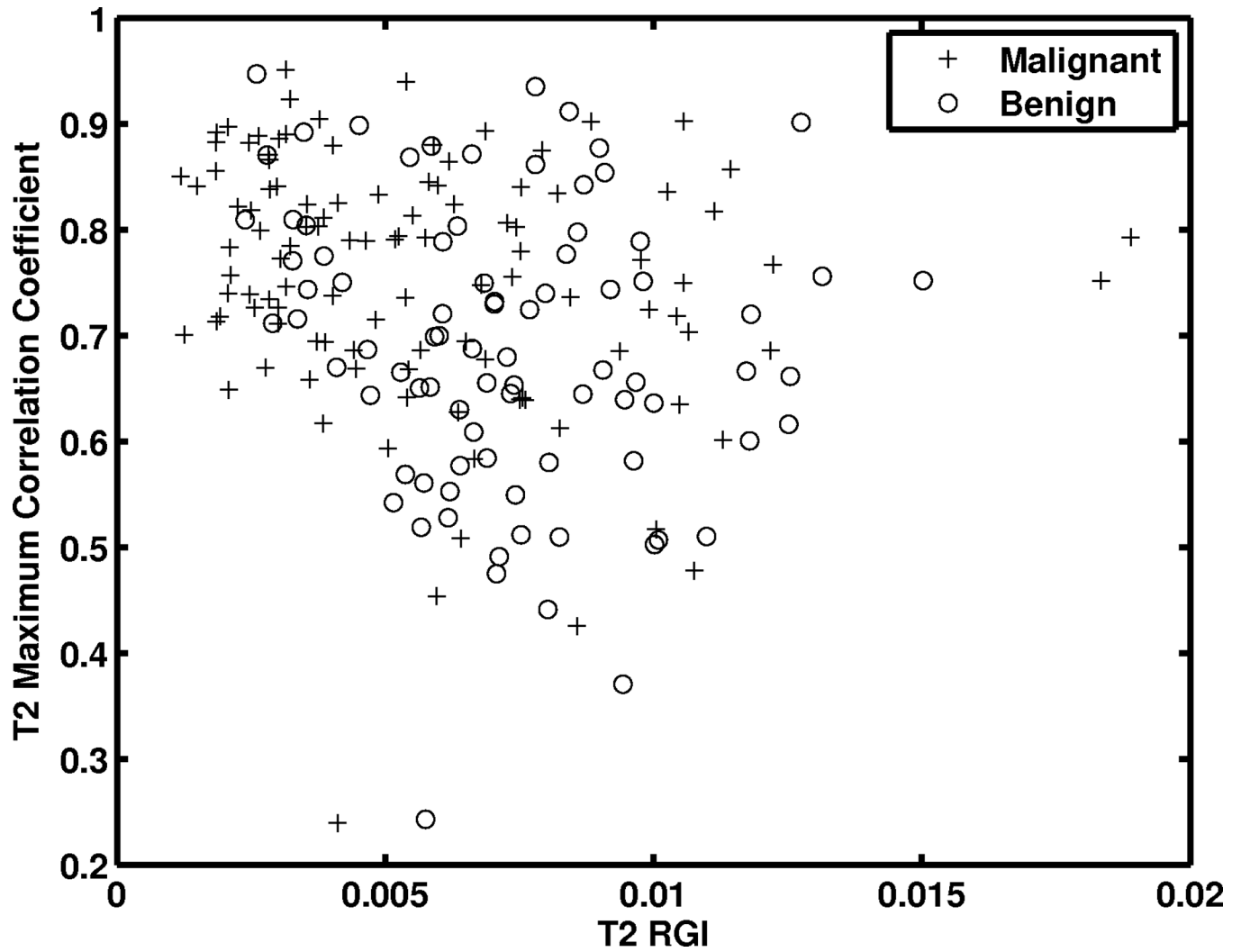


Figure 7.
Relationship between T2-weighted RGI and maximum correlation coefficient features.

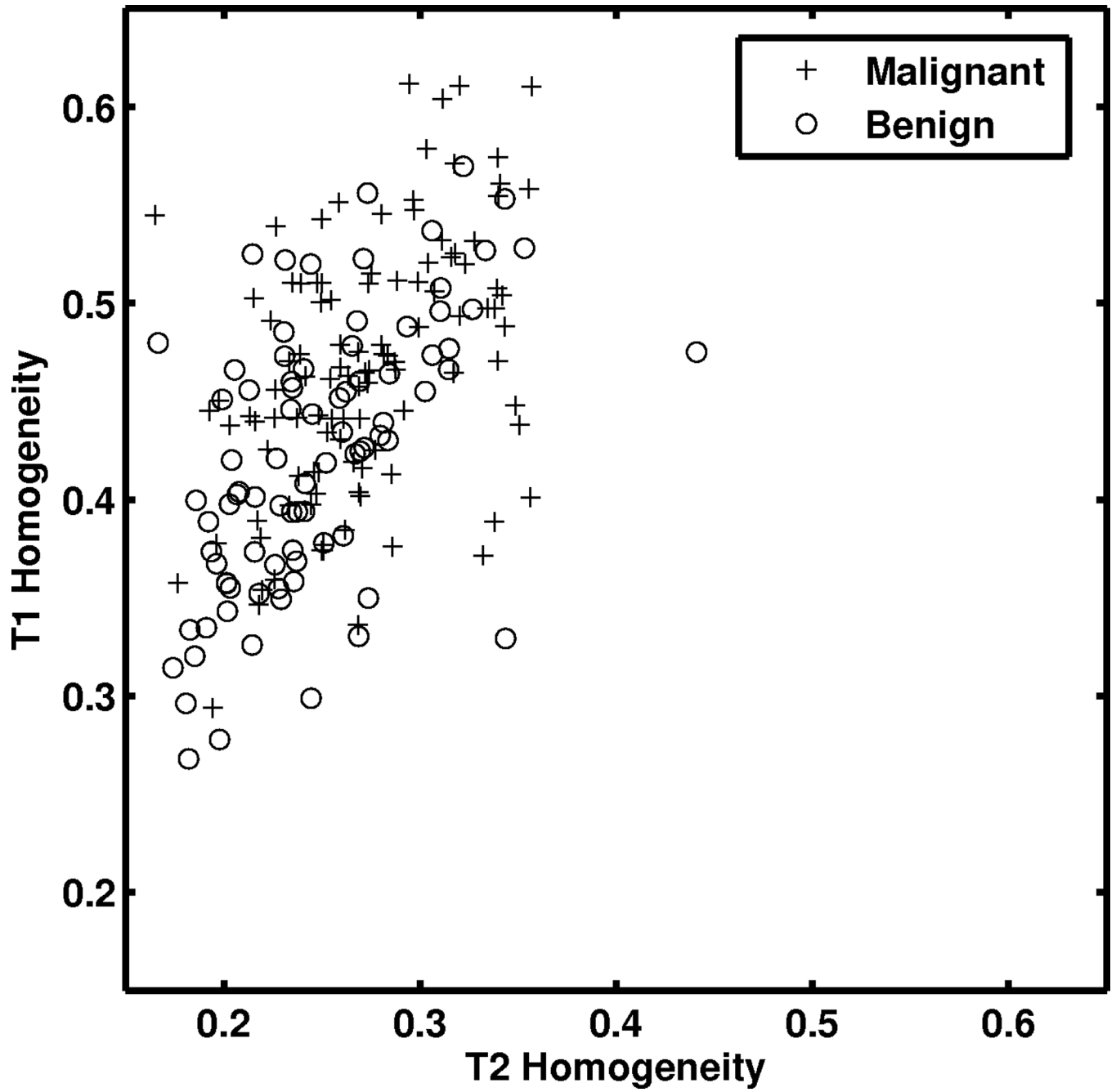


Figure 8. Relationship between T1-weighted DCE and T2-weighted values for homogeneity.

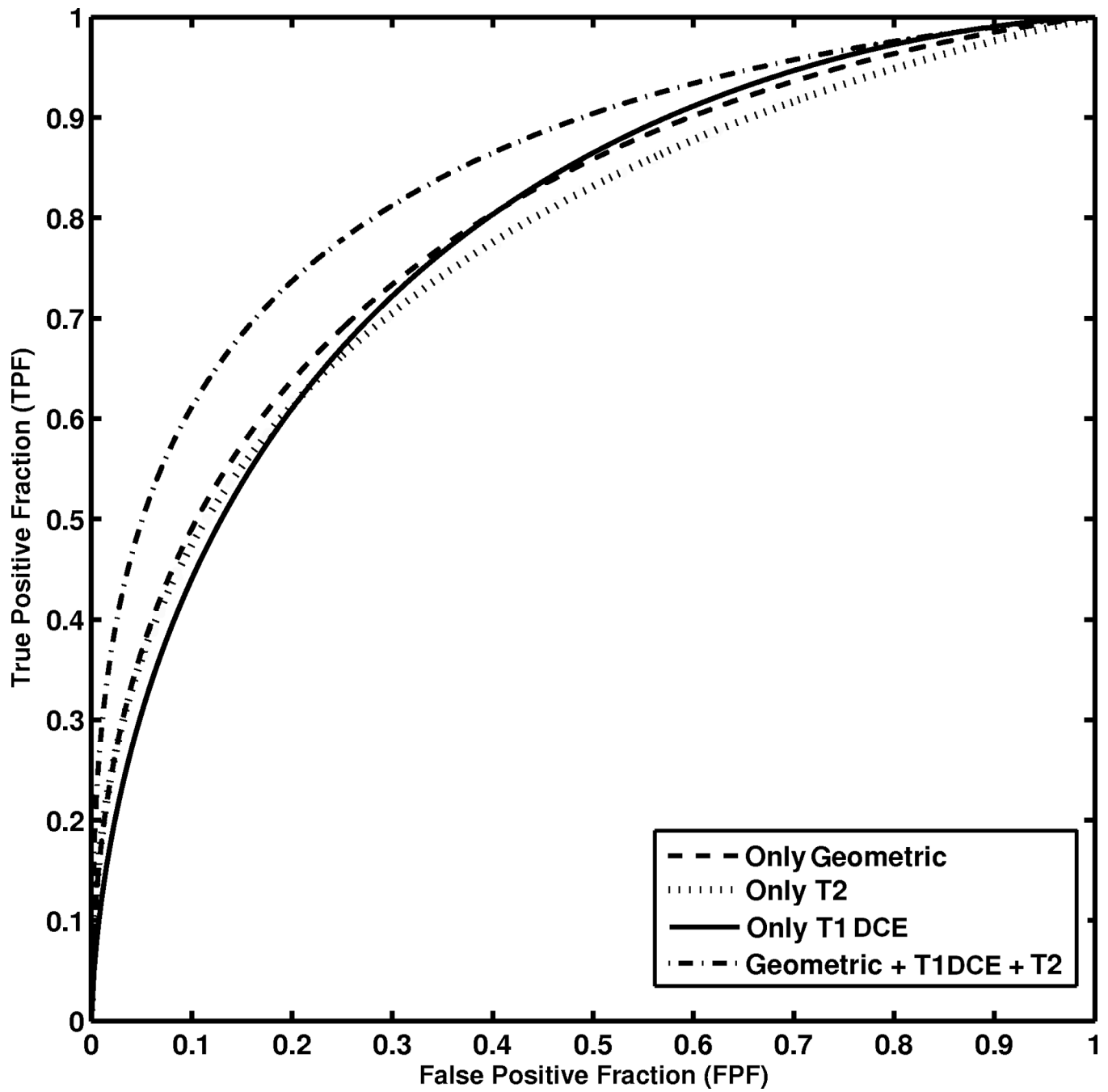


Figure 9. ROC curves for (i) considering only geometric features, (ii) considering only T1-weighted DCE features, (iii) considering only T2-weighted features, and (iv) considering all features.

Table 1

List of computer-extracted lesion features by type (texture, geometric, spiculation, kinetics, enhancement-variance kinetics) and category (T1 for T1-weighted DCE, T2 for T2-weighted, or G for geometric)

Type		Lesion features	Description	Category
Morphological – Texture ^{21,22}	T_1	Contrast	Measure of local image variations	T1, T2
	T_2	Correlation	Measure of image linearity	T1, T2
	T_3	Difference in Entropy	Measure of randomness of difference of neighboring gray-levels	T1, T2
	T_4	Difference in Variance	Measure of variations of difference of gray-levels between voxel-pairs	T1, T2
	T_5	Energy	Measure of image homogeneity	T1, T2
	T_6	Entropy	Measure of randomness of gray-levels	T1, T2
	T_7	Homogeneity	Measure of the local homogeneity	T1, T2
	T_8	Information Correlation of Measure 1	Measure of non-linear gray-level dependence	T1, T2
	T_9	Information Correlation of Measure 2	Measure of non-linear gray-level dependence	T1, T2
	T_{10}	Maximum Correlation Coefficient	Measure of non-linear gray-level dependence	T1, T2
	T_{11}	Sum Average	Measure of overall image brightness	T1, T2
	T_{12}	Sum Entropy	Measure of the randomness of the sum of gray-levels of neighboring voxels	T1, T2
	T_{13}	Sum Variance	Measure of how spread out the sum of the gray-levels of voxel-pairs is	T1, T2
	T_{14}	Variance	Measure of how spread out the gray-level distribution is	T1, T2
Geometric ²⁰	G_1	Size	Volume of lesion in cubic centimeters	G
	G_2	Sphericity	Conformity of lesion to spherical shape	G
	G_3	Irregularity	Deviation of 3D lesion surface from sphere surface	G
Morphological – Spiculation ²⁰	M_1	Margin sharpness	Mean of image gradient at lesion margin	T1, T2
	M_2	Variance of margin sharpness	Variance of the image gradient at lesion margin	T1, T2
	M_3	Radial gradient index (RGI)	How well the enhancement structures in a lesion extend in a radial pattern originating from the center of the lesion	T1, T2
Kinetics ¹⁸	K_1	Maximum Uptake	Maximum contrast enhancement	T1
	K_2	Time to Peak	Time frame at which maximum uptake occurred	T1
	K_3	Uptake Rate	Uptake rate of contrast enhancement	T1
	K_4	Washout Rate	Washout rate of contrast enhancement	T1
	K_5	Curve Shape Index	Difference between early and late enhancement	T1
	K_6	Enhancement at 1 st Post-contrast timepoint		T1

Type		Lesion features	Description	Category
	K_7	Signal Enhancement Ratio	Ratio of initial enhancement to overall enhancement	T1
Enhancement-Variance Kinetics ¹⁹	S_1	Maximum Variance of Enhancement	Maximum variance of contrast enhancement	T1
	S_2	Time to Peak	Time frame at which maximum variance occurs	T1
	S_3	Enhancement Variance Increasing Rate	Increasing rate of enhancement-variance	T1
	S_4	Enhancement Variance Decreasing Rate	Decreasing rate of enhancement-variance	T1

Table 2

Computer-selected features and diagnostic performance in which (i) only geometric features were considered, (ii) only T1-weighted DCE features were considered, (iii) only T2-weighted features were considered, and (iv) all features were considered in terms of $AUC \pm SE$ (standard error) with p -values calculated between conditions {i, ii, iii} and iv. Note that the “all features” condition corresponds to having had input all features to the feature selection algorithm.

Condition	Selected Features (single feature AUC)	AUC \pm SE	p -value (in comparison to “all features” condition)
(i) Considered only Geometric features	Irregularity (0.82) Size (0.81) Sphericity (0.67)	0.79 \pm 0.03	0.006
(ii) Considered only T1-weighted DCE features	RGI (0.78) Homogeneity (0.68) Maximum enhancement (0.50) Time to peak (0.64) Signal enhancement ratio (0.67) Enhancement-variance time to peak (0.55)	0.80 \pm 0.03	0.023
(iii) Considered only T2-weighted features	RGI (0.74) Homogeneity (0.72) Maximum correlation coefficient (0.70)	0.77 \pm 0.03	0.0014
(iv) Considered all features (Geometric, T1-weighted DCE, T2-weighted)	Irregularity (0.82) T1 RGI (0.78) T1 Enhancement-variance time to peak (0.55) T1 Signal enhancement ratio (0.67) T2 Homogeneity (0.72) T1 Maximum correlation coefficient (0.70) T2 Sum average (0.53)	0.85 \pm 0.03	